Engineering Model for Analysis of Scramjet Combustor Performance with Finite-Rate Chemistry

Maria V. Pulsonetti,* John Erdos,† and Kevin Early‡
General Applied Science Laboratories, Inc., Ronkonkoma, New York 11779

An engineering model of diffusion and reaction-limited supersonic combustion is described. The key feature of this model is that it divides the flowfield into three parallel, one-dimensional streams: 1) the fuel stream, 2) the oxidizer stream, and 3) the product stream. Fuel and oxidizer are continuously fed into the product stream in accordance with an empirical mixing model and allowed to react at a finite rate. Comparisons with experimental data for hydrogen-air combustion are presented. The model is clearly oversimplified compared to the complex two- and three-dimensional turbulent mixing and induced shock train processes known to exist in supersonic combustors. Nevertheless, it includes sufficient physics to provide reasonably good agreement with the data and enables rapid interpretation of the global features of the experiments. Accordingly, it may be useful in conceptual design studies.

Nomenclature

A = area per unit width (height)
C_p = specific heat at constant pressure
f = mixing rate parameter
G = gap height
h = enthalpy per unit mass
M = Mach number
M_i = molecular weight of species i
$M_j(N_i)$ = multiplying factor applied to jth reaction rate when species N_i is the catalytic third body
$\dot{m}$ = mass flow per unit width
n_i = moles of i per mass of i
$\bar{n}$ = number of atoms of a particular element
P = static pressure
R_o = universal gas constant
S = injection slot height
T = static temperature
u = velocity
$\dot{w}_i$ = rate of production of species i
X = streamwise coordinate
X_{cl} = cooling length
X_{lp} = length for minor constituent to be fully mixed
α_i = mass fraction of species i
γ = ratio of specific heats
δ = height of boundary layer
δ^* = displacement thickness
η = efficiency
λ = fuel/air mass flow ratio
ρ = density
ϕ = equivalence ratio
ψ = $(\rho_f u_f)/(\rho_a u_a)$

Subscripts

a = air
B = bottom
c = combustion
e = edge or inviscid conditions
f = fuel
i = initial
k = axial location index
m = mixing
stm = stoichiometric
T = top
t = total conditions
w = wall conditions
1 = conditions of stream 1
2 = conditions of stream 2
3 = conditions of stream 3

Superscript

$'$ = properties after mixing

Introduction

THE combustion process of a scramjet engine is one of the primary areas of research in the development of a hypersonic vehicle. An analysis of such a process based on solution of the Navier-Stokes equations including the effects of finite-rate chemical kinetics, viscosity, thermal and mass diffusion, and turbulence is now feasible using contemporary methods. However, it is also very costly, time consuming, and subject to the limitations of available turbulence modeling. A method that could quickly predict the overall performance of a scramjet combustor would have great practical utility for the preliminary design process, as well as for rapid interpretation of experimental data.

The engineering model we have developed, THREMX, embodies such a method. The model basically consists of three one-dimensional streams: 1) the airstream entering through the inlet, 2) the fuel stream injected into the combustor, and 3) the product stream, which air and fuel enter at a specified rate (using the mixing rate model from Ref. 1) and are allowed to react at a finite rate. The chemical rate equations are integrated over a spatial marching step independently of the fluid dynamic equations through an implicit Newton-Raphson iteration (using an adaptation of the CREK code from Ref. 2). The results are then used in the fluid dynamic equations that are integrated across the same step using Gill's version of the Runge-Kutta technique (c.f. Ref. 3). Following each step, the solution is iterated to ensure conservation of mass, momentum, and energy within each stream as well as in total.

The three-stream numerical formulation is a quasi-one-dimensional analysis of finite-rate chemically reacting flow

Presented as Paper 88-3258 at the AIAA/ASME/SAE/ASEE 24th Joint Propulsion Conference, Boston, MA, July 11-13, 1988; received Nov. 5, 1988; revision received Sept. 5, 1989; accepted for publication Sept. 12, 1989.

*Research Scientist; currently Student, University of Queensland, Mechanical Engineering Department, St. Lucia, QLD 4072, Australia. Member AIAA.

†Vice President, 77 Raynor Avenue. Associate Fellow AIAA.

‡Research Scientist; currently at GE Aircraft Engines, Cincinnati, OH 45215.

through a duct of a specified area. A schematic drawing of the flow model is shown in Fig. 1. The three streams are all at the same pressure at any given x location, but each stream has its own velocity, temperature, and composition. Stream 1 is the oxidizing stream, typically equilibrium air, although a gas of any composition can be used. Stream 2 is the fuel stream. In the present study, we have looked exclusively at hydrogen; however, the model can admit any gaseous fuel. Stream 3 is the mixing layer and is assumed to be where combustion takes place. However, the gases in all three streams can react at finite rate based on their temperature, density, and composition.

Note that, with a little imagination, the flowfield depicted in Fig. 1 can be interpreted as a duct with a flush fuel injector on one wall, half a duct with flush injectors on both walls, or half a duct with a central strut fuel injector.

Initial Conditions

The initial conditions require that the three streams be parallel and at equal pressures. This would imply that the fuel has been injected tangentially at a matched static pressure. However, vectored, three-dimensional, and/or underexpanded injectors can be handled by converting them to equivalent matched tangential injectors by use of the JETPEN code.[4,5] This code determines flow conditions downstream of injection where the fuel flow is turned parallel to the airflow and the pressure equilibrates, presumably before any significant mixing and reactions have occurred.

The JETPEN model assumes the fuel enters the combustor from an underexpanded nozzle. The code first calculates fuel conditions just downstream of a Mach disk whose position is determined by an empirical back-pressure condition. It then calculates the airflow conditions behind the interaction bow shock caused by the fuel addition. The code then begins an iteration with an initial guess on the downstream static pressure to which the two streams will expand. The fuel is assumed to expand isentropically downstream of the Mach disk and its flow area and properties are computed from the pressure. The average total pressure loss for the air across the bow shock is obtained by integrating the local total pressure loss along the shock contour, which is related to the effective height of the fuel jet using a hypersonic blunt-body approximation. Using this value plus the guessed static pressure, the flow area and properties are calculated. The pressure is iterated upon until the sum of the flow areas for the fuel stream and the airstream equals the height of the duct. Should the fuel jet be overexpanded, the fuel is assumed to expand isentropically from its plenum state (i.e., the shock losses are neglected).

The initial height, velocity, and temperature of stream 3 are selected with the intention of using stream 3 to approximate the boundary layer on the surface of the duct where injection occurs. There is an option in the code as to the calculation of these conditions. One method is to have the initial velocity of stream 3 correspond to that at the point of maximum static enthalpy in the boundary layer. To do this, the derivative of the static enthalpy with respect to the velocity is calculated from a Crocco integral relation and set equal to zero to find the maximum static enthalpy. The static enthalpy relation is

$$h = \left(\frac{h_{t_1} - h_w}{u_1}\right)u + h_w - \frac{u^2}{2} \tag{1}$$

Taking the derivative with respect to u and setting it equal to zero gives the velocity of stream 3:

$$u_3 = \frac{h_{t_1} - h_w}{u_1} \tag{2}$$

This also gives the initial temperature of stream 3 corresponding to the maximum static enthalpy in the boundary layer:

$$h_{\max}(T_3) = \frac{1}{2}\left(\frac{h_{t_1} - h_w}{u_1}\right)^2 + h_w \tag{3}$$

This approach emphasizes the temperature rise in the shear layer caused by the difference in velocities between the airstream and fuel stream as the probable autoignition source at hypersonic conditions. One problem with this approach is that at nonhypersonic conditions the enthalpy does not reach a maximum value within the boundary layer. This necessitated the other method for the calculation of the initial conditions of stream 3, which is now regarded as the preferred method. In this method, the initial velocity of stream 3 is set equal to one-half the initial velocity of stream 1, in order to approximate the average velocity in the boundary layer. The enthalpy and corresponding temperature are calculated from the Crocco integral relation:

$$h_{t_3} = h_{t_1}\frac{u_3}{u_1} + h_w\left(1 - \frac{u_3}{u_1}\right) \tag{4}$$

At hypersonic, cold wall conditions, these two methods produce the same result because the velocity at maximum static enthalpy approaches one-half the freestream value.

The initial height of stream 3 is calculated from mass conservation of the airstream. The latter is calculated using the displacement thickness of the inlet airflow. If only the boundary-layer thickness on this surface is known, e.g., from visual observations, the displacement thickness is calculated using a power law distribution of velocity in the boundary layer, which is assumed to be turbulent:

$$\frac{u}{u_e} = \left(\frac{y}{\delta}\right)^{\frac{1}{n}} \tag{5}$$

Typical values of n are 7 for subsonic flow, 5 for supersonic flow, and 3 for hypersonic flow. The density distribution is assumed to be the inverse of the enthalpy distribution:

$$\frac{\rho}{\rho_e} = \frac{h_e}{h} \tag{6}$$

The enthalpy distribution is given by the Crocco integral relation, which may be manipulated to obtain:

$$\frac{h}{h_e} = \frac{h_w}{h_e}\left(1 - \frac{u}{u_e}\right) + \frac{(\gamma_e - 1)}{2}M_e^2\frac{u}{u_e}\left(1 - \frac{u}{u_e}\right) + \frac{u}{u_e} \tag{7}$$

The above equations are substituted into the definition of displacement thickness

$$\frac{\delta^*}{\delta} = \int_0^1 \left(1 - \frac{\rho u}{\rho_e u_e}\right)\mathrm{d}\left(\frac{y}{\delta}\right) \tag{8}$$

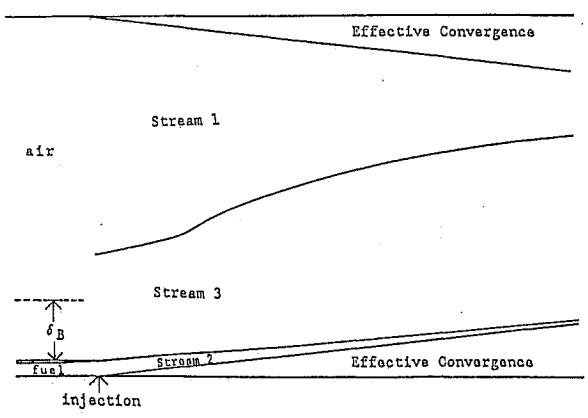

Fig. 1 Schematic of three stream mixing situation.

to obtain

$$\frac{\delta^*}{\delta} = \int_0^1 \left\{ 1 - (u/u_e) \Big/ \left[\frac{h_w}{h_e}\left(1 - \frac{u}{u_e}\right) + \frac{(\gamma_e - 1)}{2} \times M_e^2 \frac{u}{u_e}\left(1 - \frac{u}{u_e}\right) + \frac{u}{u_e} \right] \right\} d\left(\frac{y}{\delta}\right) \tag{9}$$

The displacement thickness is obtained by integrating numerically. Using this value, along with the values of q_3 and u_3, the initial height of stream 3 can be calculated from conservation of mass. The following expressions for the inlet airflow include provisions for a boundary layer on the top wall (a duct) as well as for a plane of symmetry (a free boundary):

Duct:

$$\dot{m}_a = \rho_1 u_1 (A_i - \delta_T^* - \delta_B^*) \tag{10a}$$

Free boundary:

$$\dot{m}_a = \rho_1 u_1 (A_i - \delta_B^*) \tag{10b}$$

Mass conservation can also be expressed as

Duct:

$$\dot{m}_a = \rho_1 u_1 (A_i - \delta_T^* - A_3) + \rho_3 u_3 A_3 \tag{11a}$$

Free boundary:

$$\dot{m}_a = \rho_1 u_1 (A_i - A_3) + \rho_3 u_3 A_3 \tag{11b}$$

These mass conservation relations can be equated and solved for A_3 to yield the following equation:

Duct or free boundary:

$$A_3 = \left[\frac{\rho_1 u_1 \delta_B^*}{\rho_1 u_1 - \rho_3 u_3} \right] \tag{12}$$

Note that for $U_3 \to 0$, $A_3 \to \delta_B^*$. However, in the present approximation, $A_3 > \delta_B^*$. Therefore, the effective duct height A_1 must be adjusted accordingly:

Duct:

$$A_1 = A_i + \delta_T^* - A_3 \tag{13a}$$

Free boundary:

$$A_1 = A_i - A_3 \tag{13b}$$

Mixing Process

The mixing rate is assumed to be described by a model developed by Anderson[1] for the mixing of hydrogen and air. Anderson's model specifies two mixing rates, one for tangential injection and one for normal injection, reflecting the different levels of induced turbulence associated with the differing degrees to which the fuel initially penetrates the airstream. The mixing efficiency is defined as the ratio of the mass of minor constituent (i.e., fuel for $\phi \le 1$ and air for $\phi > 1$) that has been mixed to the available mass of minor constituent. The tangential injection rate predicts the mixing efficiency to be a linear function of the length required for the minor constituent to be fully mixed (X_{lp}).

$$\eta_{m_{0\,\deg}} = \frac{X}{X_{lp}} \tag{14}$$

The normal injection mixing rate is defined by the following equation:

$$\eta_{m_{90\,\deg}} = 1.01 + 0.176 \ln\left(\frac{X}{X_{lp}}\right) \tag{15}$$

For injection angles between 0 and 90 deg, a linearly weighted average of these two values is used. For both models, X_{lp} is empirically determined to be the following:

$$X/X_{lp} = 0.179 e^{1.72\phi}, \qquad \phi \le 1 \tag{16a}$$

$$= 3.333 e^{-1.204\phi}, \qquad \phi > 1 \tag{16b}$$

$$X_{lp} = fG \tag{16c}$$

where G is the effective (inviscid) duct height and f is an empirical mixing rate constant. The mass transfer of the minor constituent into the mixing stream is given by

$$(\Delta \dot{m}_f)_k = \eta_m \dot{m}_{f_{\text{initial}}} - \sum_{j=1}^{k-1} (\Delta \dot{m}_f)_j \qquad \phi \le 1 \tag{17a}$$

$$(\Delta \dot{m}_a)_k = \eta_m \dot{m}_{a_{\text{initial}}} - \sum_{j=1}^{k-1} (\Delta \dot{m}_a)_j \qquad \phi > 1 \tag{17b}$$

while the corresponding transfer of the major constituent into the mixing stream is

$$(\Delta \dot{m}_a)_k = (\Delta \dot{m}_f)_k / [\phi_{\text{mix}} \lambda_{\text{stm}}] \qquad \phi \le 1 \tag{18a}$$

$$(\Delta \dot{m}_f)_k = (\Delta \dot{m}_a)_k \phi_{\text{mix}} \lambda_{\text{stm}} \qquad \phi > 1 \tag{18b}$$

where λ_{stm} is the stoichiometric fuel-oxidizer ratio and ϕ_{mix} is the specified equivalence ratio of stream 3, which has been assumed equal to 1 in this model, i.e., the fuel and oxidizer are entrained into stream 3 in stoichiometric proportions. When the minor constituent stream is depleted, the major constituent stream is assumed to continue to mix at the rate it was mixing when the minor constituent stream ran out, until it too is depleted. At this point, stream 3 will have attained the overall equivalence ratio provided by the fuel injector mass flow rate and the calculation will proceed as a fully mixed, single-stream tube.

The mass entering the mixing stream from the airstream and fuel stream on each marching step has different properties (i.e., temperature, velocity, etc.). Therefore, the properties after mixing are different than the properties before mixing. In effect, the model treats the chemical changes, inviscid changes, and changes due to mixing as three sequential processes.

Streams 1 and 2 are only allowed to lose mass during the mixing process; therefore, the total enthalpy per unit mass of streams 1 and 2 will remain constant. The composition of stream 3 changes during the mixing process due to the added mass. Its new composition is calculated from mass averages as follows:

$$\alpha_3' = \frac{\dot{m}_3 \alpha_{3_i} + \Delta \dot{m}_a \alpha_{2_i} + \Delta \dot{m}_f \alpha_{2_i}}{\dot{m}_3 + \Delta \dot{m}_a + \Delta \dot{m}_f} \tag{19}$$

The total enthalpy per unit mass is likewise calculated from a mass average as follows:

$$h_3'(T_3') + \frac{u_3'^2}{2} = \frac{\dot{m}_3 [h_3(T_3) + u_3^2/2] + \Delta \dot{m}_a [h_1(T_1) + u_1^2/2]}{\dot{m}_3 + \Delta \dot{m}_a + \Delta \dot{m}_f} + \frac{\Delta \dot{m}_f [h_2(T_2) + u_2^2/2]}{\dot{m}_3 + \Delta \dot{m}_a + \Delta \dot{m}_f} \tag{20}$$

From the laws of conservation of mass and momentum for each stream, including transfers between streams, one can obtain six more equations. Hence, we have nine equations and nine unknowns, namely P', u_1', u_2', u_3', T_1', T_2', T_3', and two of the three areas, since we know that the sum of the three areas must equal the specified area. Therefore, the solution is determinate. An iterative scheme is used due to the nonlinear dependence of enthalpy on temperature.

Inviscid Processes

After the mixing is complete at a particular x location, the solution is advanced downstream using a set of quasi-one-dimensional Euler equations for each stream. A pressure at a new x location is guessed and each stream is advanced using Gill's method of the Runge-Kutta fourth-order integration technique[3] yielding a new velocity, temperature, density, and area, while the composition of each stream is allowed to vary through a finite-rate chemical process.[2] The sum of the three areas calculated is compared to the specified area at that x location, and the guessed pressure is adjusted until these areas match.

The governing equations used for solution advancement are the following: 1) global continuity, 2) species continuity, 3) conservation of momentum, 4) conservation of energy, and 5) equation of state. The species continuity equation is solved separately from the others in conjunction with the conservation of energy.

Combustion Efficiency

The combustion efficiency is defined as the fraction formed by the number of atoms of reactant in the minor constituent that have already reacted to water divided by the total number of atoms of reactant in all species. In other words, it is the ratio of the amount of water present to the theoretical maximum that could be formed (at room temperature). Hence,

$$\eta_c = \frac{2n_{H_2O}}{\bar{n}_H} \qquad \phi \le 1$$

$$= \frac{n_{H_2O}}{\bar{n}_O} \qquad \phi > 1 \qquad (21)$$

where n_i represents the moles of i per mass of the mixture and

$$\bar{n}_H = n_H + 2n_{H_2} + 2n_{H_2O} + n_{OH} + \cdots \qquad (22)$$

$$\bar{n}_O = n_O + 2n_{O_2} + n_{H_2O} + n_{OH} + \cdots \qquad (23)$$

Note that this is a convenient definition for the present purposes since it is independent of the final thermochemical state of the combustion products. However, it is not the same as the more commonly used definition (c.f. Ref. 6), which is based on the ratio of heat released (or temperature rise) to the maximum heat release (or temperature rise) at the chemical equilibrium end state. At high temperatures, the presently defined value will be less than the more commonly defined value due to dissociation of the water and production of nitric oxide.

Chemical Kinetics Model

The chemical kinetics package used in THREMX was derived from the model of Rogers and Schexnayder.[6] Their calculations were made for pressures of 0.2–4.0 atm, temperatures from 850 to 2000 K, and equivalence ratios from 0.2 to 2.0. Their model included 60 reactions involving 20 species of hydrogen, oxygen, and nitrogen as well as third-body efficiencies of five different species in seven reactions.

The chemical kinetics model in THREMX contains 25 of their 60 reactions involving 11 of their 20 species plus argon for a hydrogen, oxygen, nitrogen, argon system. A complete set of the reactions, reaction rate constants, and third-body efficiencies can be found in Table 1.

Comparisons with Data

The first comparison was made with the data of Burrows and Kurkov.[7] Their experiments consisted of parallel injec-

Table 1 Hydrogen-oxygen-nitrogen reaction model with third-body efficiencies
rate constant[a]: $K = AT^N e^{\text{activation energy}/R_o T}$

Reaction number	Reaction	log A	N	Activation energy/R_o
1	O2 + M ↔ O + O + M	15.9	−1.0	59,300
2	H2 + M ↔ H + H + M	15.7	−1.0	52,000
3	H2O + M ↔ OH + H + M	18.7	−1.5	59,400
4	H + O2 + M ↔ HO2 + M	9.36	0.0	−403
5	NO2 + M ↔ NO + O + M	13.0	0.0	32,700
6	NO + M ↔ N + O + M	15.6	−1.0	75,300
7	O + H + M ↔ OH + M	12.9	−1.0	0.0
8	H2O + O ↔ OH + OH	10.8	0.0	9,060
9	H2 + OH ↔ H2O + H	10.3	0.0	2,600
10	O2 + H ↔ OH + O	11.3	0.0	8,460
11	H2 + O ↔ OH + H	10.9	0.0	5,590
12	H2 + O2 ↔ OH + OH	10.0	0.0	21,600
13	H + HO2 ↔ H2 + O2	10.4	0.0	350
14	H2 + O2 ↔ H2O + O	10.6	0.0	25,400
15	H + HO2 ↔ OH + OH	11.4	0.0	950
16	H2O + O ↔ H + HO2	8.76	0.5	28,700
17	O + HO2 ↔ OH + O2	10.7	0.0	503
18	OH + HO2 ↔ O2 + H2O	10.5	0.0	0.0
19	H2 + HO2 ↔ H2O + OH	10.3	0.0	12,600
20	O + N2 ↔ NO + N	10.7	0.0	37,900
21	H + NO ↔ OH + N	11.2	0.0	24,500
22	O + NO ↔ O2 + N	6.18	1.0	19,500
23	NO2 + H ↔ NO + OH	11.5	0.0	740
24	NO2 + O ↔ NO + O2	10.0	0.0	302
25	HO2 + NO ↔ NO2 + OH	9.48	0.5	1,210

Third-body efficiencies

Reaction 1	Reaction 2	Reaction 3	Reaction 4
$M_1(O_2) = 4$	$M_2(H) = 5$	$M_3(H_2O) = 6$	$M_4(H_2) = 2$
$M_1(O) = 10$	$M_2(H_2) = 2$		$M_4(H_2O) = 13$
$M_1(H_2O) = 2$	$M_2(H_2O) = 8$		

[a] T is in units of Kelvin. K is in units of m³/kg mole/s for second-order reactions and in units of m⁶/kg mole²/s for third-order reactions.

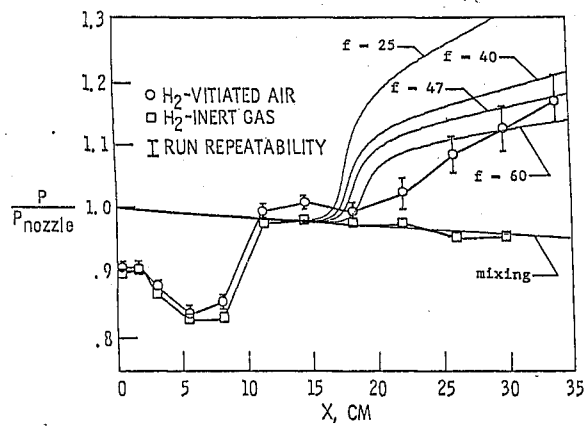

Fig. 2 Comparisons of pressure distributions for mixing and combustion runs of various mixing rate factors (f) with Burrows and Kurkov experimental data.

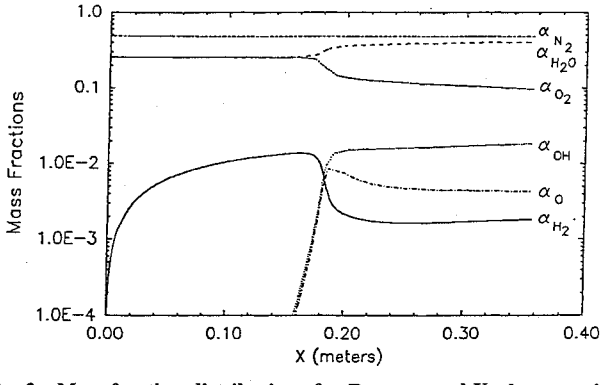

Fig. 3 Mass fraction distributions for Burrows and Kurkov reacting run with mixing rate factor of 47.

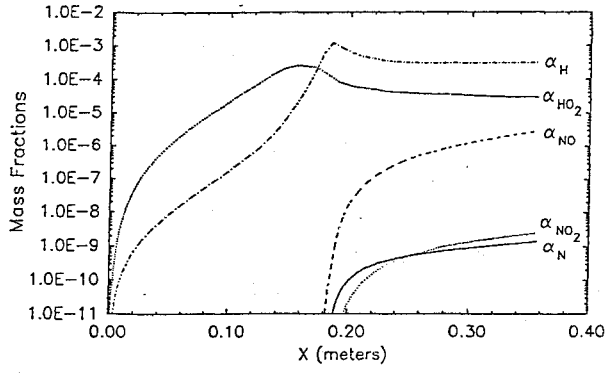

Fig. 4 Mass fraction distributions for Burrows and Kurkov reacting run with mixing rate factor of 47.

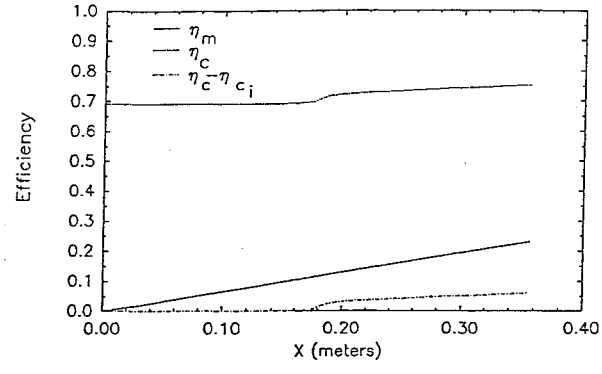

Fig. 5 Mixing and combustion efficiencies for Burrows and Kurkov reacting run with mixing rate factor of 47.

tions of hydrogen into a Mach 2.44 vitiated airstream in a diverging duct. The airstream was at a pressure of 1 atm and a temperature of 1270 K. The fuel was injected sonically at nearly matched pressure and a total temperature of 300 K.

The first calculation was done for an inert mixing run where hydrogen was injected into a vitiated nitrogen stream. (All of the oxygen initially in the stream was fully consumed in the combustion process by which the nitrogen was heated.) The divergence of the duct was decreased until the pressure rise matched the experimental data. This effective convergence of the walls accounts for the growth of the boundary-layer displacement thickness. Once the effective convergence was known, we reran the model for the combustion conditions assuming that the heat release would not significantly alter the boundary-layer properties. Figure 2 shows the comparison of the experimental pressure distribution on the lower wall and our results. The upper wall was not instrumented.

An experimental study by Parthasarathy and Zakkay[8] produced the following film cooling correlation for hydrogen as the coolant injected into a Mach 6 air mainstream:

$$X_{cl} = 1100.0\, S\psi^{0.8} \tag{24}$$

If the cooling length is equated to the length for the minor constituent to be fully mixed X_{lp} from Eq. (16a) for $\phi \le 1$, the resulting equation can be solved for f:

$$f = 6145.25\, \frac{S}{G}\, \frac{[\phi \lambda_{stm}(G/S)]^{0.8}}{e^{1.72\phi}} \tag{25}$$

For the Burrows and Kurkov test conditions, the mixing rate factor was calculated to be 47. This is reasonably close to the value originally proposed by Anderson, $f = 60$, based on an independent correlation of experimental data and theoretical calculations of fuel mixing. The mixing and combustion runs were made varying the mixing rate factor. The values used were 25, 40, 47, and 60. Changes in the mixing rate factor had no effect on the pressure distribution for the mixing run; however, they had a profound impact on the pressure distribution for the combustion runs (see Fig. 2). The mixing rate factor obtained by equating the cooling length correlation to the mixing length correlation ($f = 47$) seemed to agree best with the surface pressure data, which is considered the best available diagnostic for overall heat release. Therefore, this value was used for all remaining calculations.

The mass fraction distributions of the product stream for the combustion run can be found in Figs. 3 and 4. Notice that the initial water mass fraction is high, approximately the same value as the initial mass fraction of diatomic oxygen. This is typically the case with vitiated air. The sharp decrease in diatomic hydrogen at about $x = 0.17$ m corresponds to ignition of the fuel. Notice also the sudden decrease in atomic oxygen mass fraction and the sudden increase in water and nitric oxide mass fraction just after ignition, as the hydroxyl radical and nitrogen are attacked by the available atomic oxygen. At the combustor exit, the mass fraction of nitric oxide is still increasing indicating that the flow has not yet reached equilibrium.

Figure 5 shows the mixing and combustion efficiencies. Since the test gas for these experiments is vitiated air, the combustion efficiency, as defined earlier, has an initial value $\eta_{ci} = 0.6917$ due to the water vapor in the oxidizer stream. Therefore, the difference $\eta_c - \eta_{ci}$ is also plotted in Fig. 5 to indicate the extent to which the injected fuel is burned. Again, note the sudden increase in combustion efficiency at $x = 0.17$ m. However, for $x > 0.20$ m, it becomes clear that the reaction efficiency is lagging the mixing efficiency. The rate at which they diverge is a function of pressure and temperature, as is the asymptotic value that η_c will achieve. Note in Figs. 3

and 4 the formation of radicals such as OH, NO, and HO_2, which tie up both the available oxidizer and fuel. Recall that before the fuel is fully mixed ($\eta_m < 1$) it is continuously being added to the mixing stream, and for nonequilibrium conditions, the combustion process cannot keep up with the mixing process.

Profiles of Mach number and total temperature at the exit of the combustor for both the mixing and combustion runs can be found in Figs. 6 and 7. Note that $y = 0$ corresponds to the injection side of the combustor and that our results do not begin at $y = 0$ due to our displacement of the surface to account for the boundary layer. From these figures, one can see that although the present model, using three one-dimensional streams, cannot reproduce lateral distributions of flow properties that actually occur in the presence of turbulent mixing and combustion, the mean value in each of these regions shows satisfactory agreement with our model. Hence, our model reproduces certain basic features such as the growth of the mixing layer due to heat release. Although the model is clearly an oversimplification of the flowfield, it does retain sufficient physics to assist in the interpretation of experimental data and, therefore, in preliminary design work.

The transverse volume fraction profile of diatomic hydrogen, water, diatomic nitrogen, and diatomic oxygen can be found in Figs. 8a–8d, respectively. Again, there is general agreement with the mean values and those calculated by THREMX.

Another comparison was made with the tests recently performed in the shock tunnel at Calspan.[9] In these experiments, the combustion channel had constant area. A typically thick hypersonic inlet boundary layer was generated by a sharp flat-plate forebody on one side of the model (the body side). The other side (the cowl side) had no initial boundary layer. Pure mixing data were obtained by using nitrogen as the test gas in the shock tube. Combustion data were obtained using air as the test gas. Hydrogen was the fuel in both cases. The height of the combustion channel was variable. The span was 14 in. (0.36 m).

The first case analyzed was a mixing run and combustion run for a duct height of 1 in. The flow properties at the inlet to the combustor are given in Table 2. Fuel was injected sonically at an angle of 45 deg relative to the airstream through a set of closely spaced discrete orifices on the duct wall. The JETPEN program, which takes into account the effects of nonparallel injection, was used to determine the properties just after injection where the pressure of the fuel and airstreams equilibriates. The properties just after injection for the mixing run can be found in Table 2. The convergence of the duct was adjusted until the pressure rise matched the experimental values. This corresponded to a 47% decrease in flow area at the combustor exit. The plot of the pressure distribution for the mixing run can be found in Fig. 9. Note that x is measured from the leading edge of the forebody. The cowl leading edge is at 0.86 m and the fuel injectors are at $x = 0.99$ m.

The corresponding combustion run was then analyzed using the same duct convergence. The fluid dynamic properties are presented in Table 2. A comparison of the experimental and theoretical pressure distributions can be found in Fig. 10. The agreement is generally quite good. The chemical composition distribution of the mixing stream is shown in Fig. 11. Note that ignition occurs at about $x = 1.15$ m characterized by the sharp decrease in hydrogen mass fraction. This can also be seen in Fig. 10 where the pressure suddenly begins to climb. It can also be seen in the plot of mixing and combustion efficiency vs x (Fig. 12), i.e., the sudden increase in combustion efficiency at $x = 1.15$ m. From Fig. 11, it can be seen that the reaction has not yet gone to completion at the end of the combustor channel, $x = 1.37$ m. This is also evident in Fig. 12 where it shows that the mixing and combustion efficiencies are still rising steadily. It is also clear from Fig. 12 that the reaction process is lagging the mixing process. As in the previous example, this is due to a combination of factors, including the effect of the subatmospheric pressure on the rate of reaction and, as can be seen from Fig. 11, the relatively large amount of hydroxide and nitric oxide that are formed, thus tying up oxygen atoms otherwise available to combine with hydrogen radical to form water.

Another comparison with the shock tunnel data was made for a 3/4-in. combustor height using the same 45-deg injectors. The JETPEN code, again, was used to determine the properties just after injection. Flow properties are given in

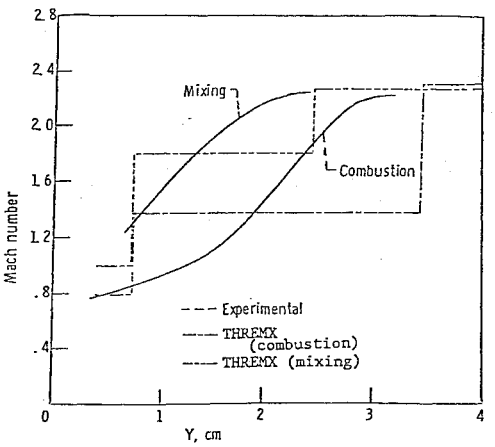

Fig. 6 Comparison of Mach number profiles with Burrows and Kurkov computed values and experimental data.

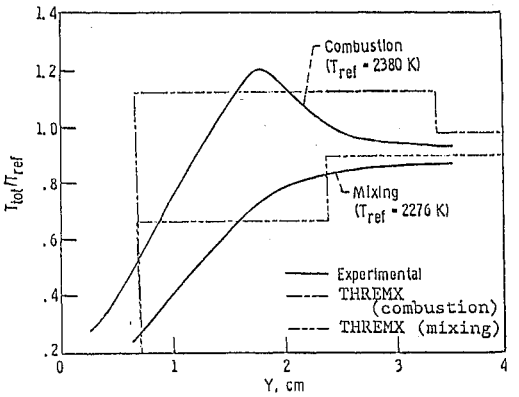

Fig. 7 Comparison of total temperature profiles with Burrows and Kurkov computed values and experimental data.

Table 2 Shock tube flow properties

Duct height, in.	Run type	Preinjection: Air properties M	P, atm	T, K	Preinjection: Fuel properties M	P_f, atm	T_f, K	Post injection: P, Pa	T_1, K	U_1, m/s	A_1, m	T_2, K	M_2	A_2, m
1	Mixing	4.2	0.45	1000	1.0	9.9	470	40,600	1030	2480	1.95E-2	188	2.67	9.94E-4
	Combustion							38,800	1110	2560	1.97E-2	186	2.74	9.22E-4
3/4	Mixing	4.2	0.45	1017	1.0	5.8	470	43,400	1180	2630	1.35E-2	219	2.34	7.29E-4
	Combustion							44,200	1160	2570	1.36E-2	223	2.34	7.59E-4

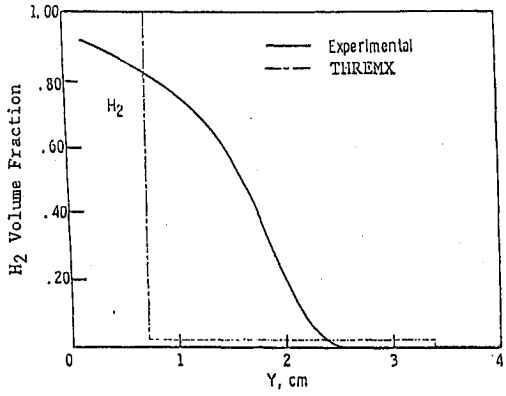

Fig. 8a Comparison of H_2 volume fraction profile with Burrows and Kurkov computed values and experimental data.

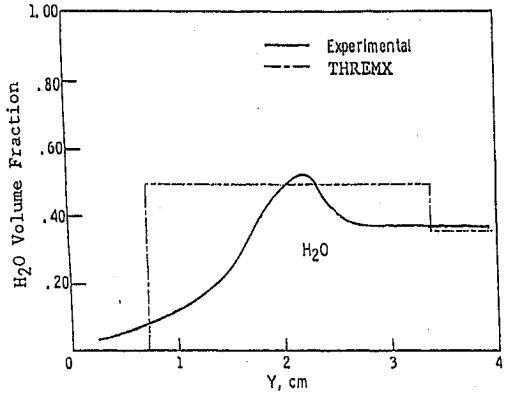

Fig. 8b Comparison of H_2O volume fraction profile with Burrows and Kurkov computed values and experimental data.

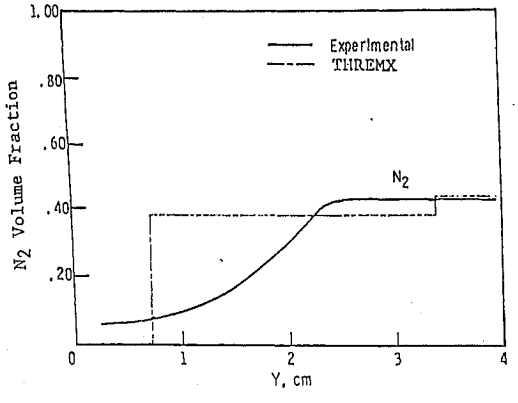

Fig. 8c Comparison of N_2 volume fraction profile with Burrows and Kurkov computed values and experimental data.

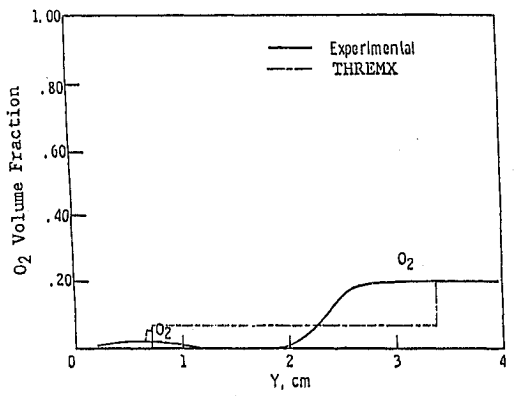

Fig. 8d Comparison of O_2 volume fraction profile with Burrows and Kurkov computed values and experimental data.

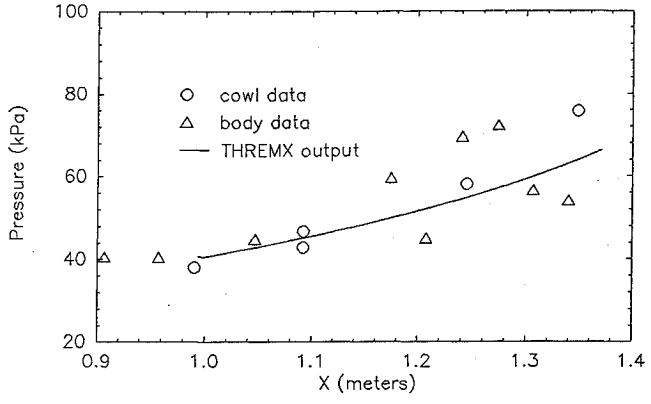

Fig. 9 Comparison of pressure distribution for Calspan mixing run with 1-in. duct height (run no. 21).

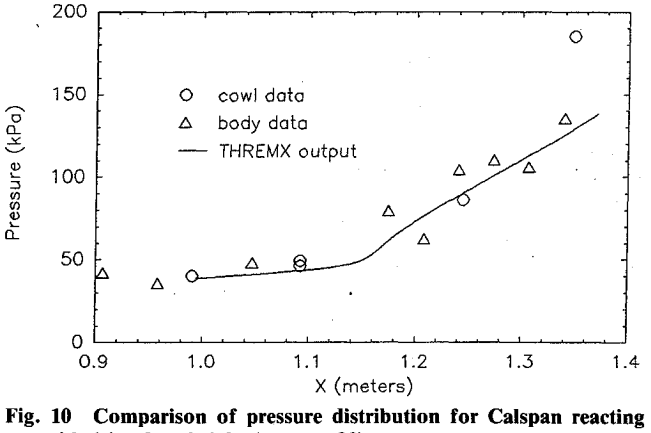

Fig. 10 Comparison of pressure distribution for Calspan reacting run with 1-in. duct height (run no. 20).

Table 2. The duct had to be converged 51% to take into account the growth of the boundary-layer displacement thicknesses on the upper and lower surfaces of the duct. The plot of the pressure distribution for the mixing run can be found in Fig. 13.

The corresponding combustion run was then examined with the same convergence. The flow properties can be found in Table 2. The pressure distribution comparison with the experimental data can be found in Fig. 14. Note again the good agreement between the experimental pressure distribution and the pressure distribution predicted with the THREMX model. Figure 15 shows the chemical composition distribution of the mixing stream. Ignition occurs at about $x = 1.06$ m, sooner than for the 1-in. combustor height primarily because of the higher static pressure. The mixing and combustion efficiency distribution can be found in Fig. 16.

Discussion

In the present study, the boundary-layer growth has been assumed to be unaffected by combustion, so that the experimental rate of pressure rise can be used to estimate the rate of fuel-air mixing and combusion. However, in an important advance over prior studies of this type, the flowfield has been modeled by three streams (air, fuel, and combustion products) with finite-rate chemical reactions. The rate of mixing between the streams has been based on two simple, heuristic models proposed by Anderson, one for normal injection and one for tangential injection, which contains a single mixing rate constant for stoichiometric mixtures and multiplying factors for nonstoichiometric cases.

The axial pressure rise in a duct due to mixing of parallel, inert streams is found to be relatively insensitive to the axial

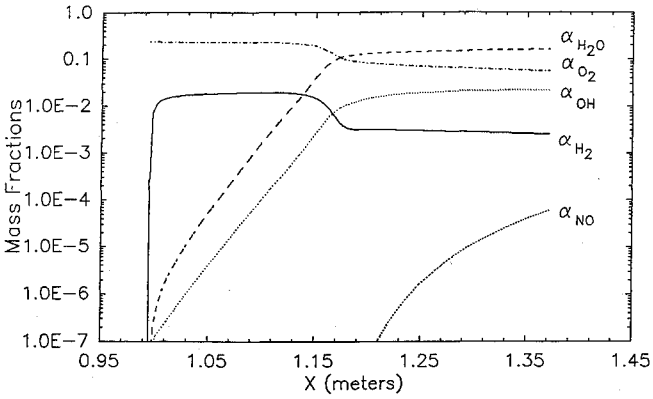

Fig. 11 Mass fraction distribution for Calspan reacting run with 1-in. duct height (run no. 20).

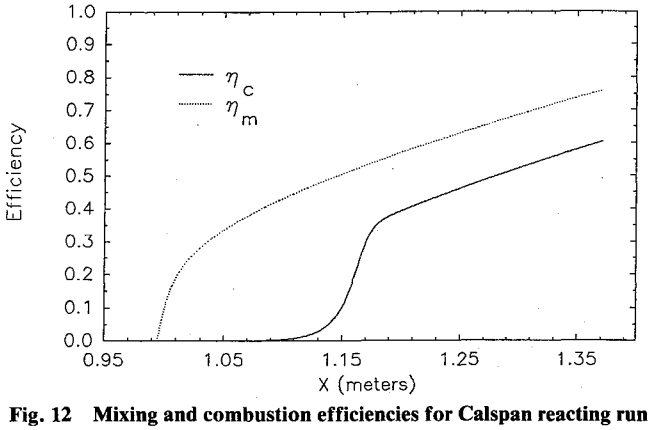

Fig. 12 Mixing and combustion efficiencies for Calspan reacting run with 1-in. duct height (run no. 20).

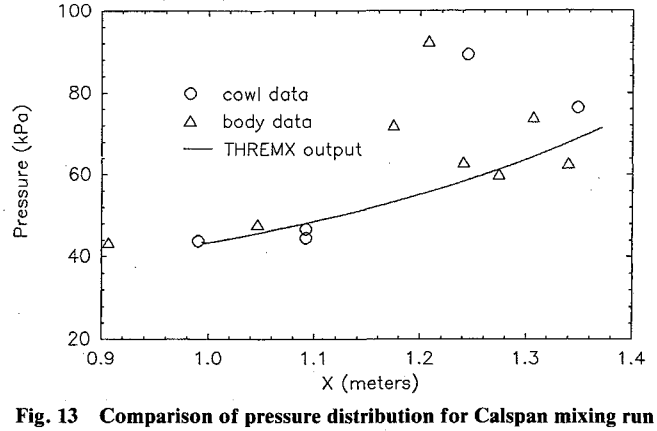

Fig. 13 Comparison of pressure distribution for Calspan mixing run with ¾-in. duct height (run no. 31).

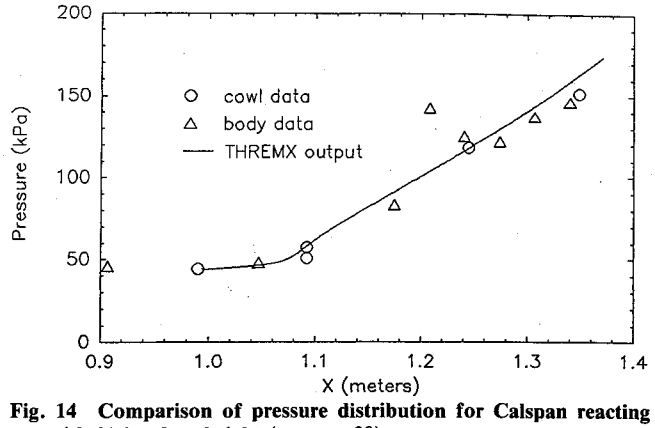

Fig. 14 Comparison of pressure distribution for Calspan reacting run with ¾-in. duct height (run no. 30).

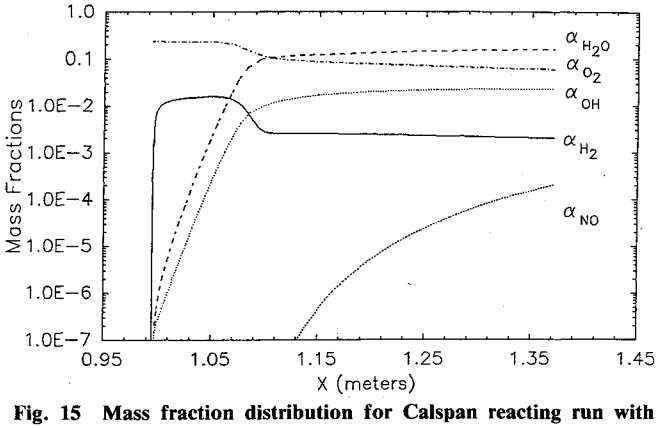

Fig. 15 Mass fraction distribution for Calspan reacting run with ¾-in. duct height (run no. 30).

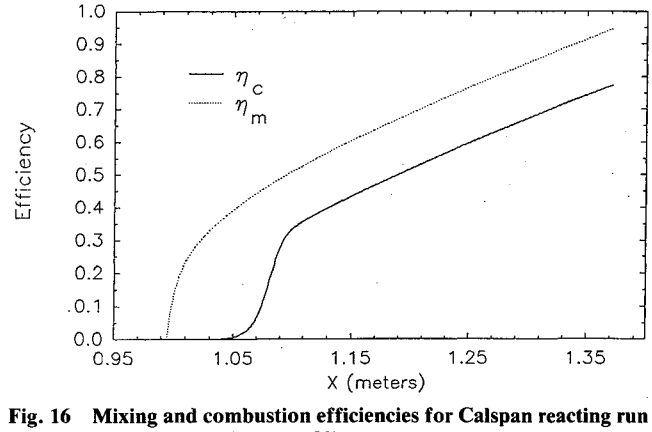

Fig. 16 Mixing and combustion efficiencies for Calspan reacting run with ¾-in. duct height (run no. 30).

rate of mixing, but it is sensitive to boundary-layer growth along the duct walls. Therefore, data from inert mixing experiments can be used to estimate boundary-layer growth, which is not included in the present analytical model.

A mixing rate constant of 25 produces reasonable agreement with the height of the mixing layer measured by Burrows and Kurkow at the end of their duct, but produces too fast a rate of pressure rise along the duct. This may be a consequence of the assumption in the present model that the pressure is constant in the transverse direction rather than propagating along Mach lines. On the other hand, a mixing rate constant of 60, as proposed by Anderson (for a somewhat different flow situation), produces too slow a rate of pressure rise. A value of 47 is proposed herein to produce the best overall agreement with pressure rise data, which is the primary experimental diagnostic for combustion efficiency. Note, however, that the Burrows and Kurkov experiments were performed for very fuel-lean conditions.

Generally, good agreement is found with the experimental data recently obtained in the Calspan shock tunnel at near stoichiometric conditions using the same mixing rate constant of 47.

It is worth emphasizing that, although Anderson's mixing model[1] was designed for normal or tangential injection of fuel from a strut, it appears to work very well for vectored wall injection of fuel (using the JETPEN code) with only a modest change to the coefficient in his model. It is also important to note that the same empirical mixing constant appears to work

well for both the Mach 2.4 and Mach 4.2 experiments. Additionally, the model performs satisfactorily for hydrogen-vitiated air as well as hydrogen-air combustion.

Conclusions

It is concluded that, although the THRMX code does not provide a detailed two dimensional solution, it does provide a quick and inexpensive analysis of overall heat release characteristics that compare very well with experimental data. Comparisons with transverse surveys of temperature, Mach number, and composition indicate that the model does embody the essential physics of diffusion controlled hypersonic-scramjet combustor flowfields.

The empirical mixing model, which depends only on duct height, fuel injection angle, and fuel equivalence ratio, provides satisfactory agreement with data taken at airflow Mach numbers of 2.4 and 4.2 and sonic fuel injection. This suggests that, at least over this range, airflow Mach number is not a first-order parameter affecting the rate of fuel-air mixing.

Acknowledgments

Portions of this work were supported by Pratt and Whitney Aircraft Co., West Palm Beach, FL, and the National Aero-Space Plane Joint Program Office, Wright-Patterson AFB, OH.

References

[1]Northam, G. B., and Anderson, G. Y., "Supersonic Combustion Ramjet Research at Langley," AIAA Paper 86-0159, Jan. 1986.

[2]Pratt, D. T., "Calculation of Chemically Reacting Flows with Complex Chemistry," *Studies in Convection Theory, Measurement and Applications,* edited by B. E. Launder, Vol. 2, Academic, New York, 1977.

[3]Abramowitz, M., and Stegan, I., *Handbook of Mathematical Functions,* Dover, New York, 1965.

[4]Billig, F. S., Orth, R. C., and Lasky, M. "A Unified Analysis of Gaseous Jet Penetration," *AIAA Journal,* Vol. 9, No. 6, 1971, pp. 1048–1058.

[5]Posillico, A., "Description of the Gaseous Jet Penetration (JET-PEN) Code," General Applied Science Lab., Ronkonkoma, NY, Interoffice Memo, June 1986.

[6]Rogers, C. R., and Schexnayder, C. J., Jr., "Chemical Kinetic Analysis of Hydrogen-Air Ignition and Reaction Times," NASA TP-1856, July 1981.

[7]Burrows, M. C., and Kurkov, A. P., "Analytical and Experimental Study of Supersonic Combustion of Hydrogen in a Vitiated Airstream," NASA TMX-2828, 1973.

[8]Parthasarathy, K., and Zakkay, V., "An Experimental Investigation of Turbulent Slot Injection at Mach 6," *AIAA Journal,* Vol. 8, No. 7, 1970.

[9]Orth, R. C., Erdos, J. I., Sanlorenzo, E., Hoose, K., Pulsonetti, M., Wittliff, C., and Padova, C., "Preliminary Data Report for Parametric Combustor Experiments Conducted in the Calspan Shock Tunnel," Vol. 1, NASP CR-1015, May 1988.